RMetS
Royal Meteorological Society

Modeling the effects of dust-radiative forcing on the movement of Hurricane *Helene* (2006)

Shu-Hua Chen,[a]* Yi-Chin Liu,[b] Terrence R. Nathan,[a] Christopher Davis,[c] Ryan Torn,[d] Nicholas Sowa,[a] Chao-Tzuen Cheng[e] and Jen-Ping Chen[f]

[a]*Department of Land, Air, and Water Resources, University of California, Davis, USA*
[b]*Pacific Northwest National Laboratory, Richland, WA, USA*
[c]*Mesoscale and Microscale Meteorology Laboratory, National Center for Atmospheric Research, Boulder, CO, USA*
[d]*Department of Atmospheric and Environmental Sciences, University at Albany, State University of New York, USA*
[e]*National Science and Technology Center for Disaster Reduction, New Taipei City, Taiwan*
[f]*Department of Atmospheric Sciences, National Taiwan University, Taipei, Taiwan*

*Correspondence to: S.-H. Chen, Department of Land, Air, and Water Resources, University of California, One Shields Avenue, Davis, CA 95616, USA. E-mail: shachen@ucdavis.edu

The influence of direct dust-radiative forcing on the movement and track of Hurricane *Helene* (2006) is examined numerically using the Weather Research and Forecasting dust model. Numerical simulations show that the model-generated dust plume modifies the thermal field, causing a clockwise turning of the vertical shear surrounding the plume, which changes the deep layer steering flow. The change in the steering flow modifies *Helene*'s moving speed and direction as it transits the plume. As *Helene* exits the plume, it has a different trajectory than it would have had in the absence of dust-radiative forcing. Consequently, the difference in the tracks with and without dust-radiative forcing continues to grow with distance from the plume. The dust-induced changes in temperature and wind together cause *Helene*'s modeled storm track to be in closer agreement with the observed track; the dust-radiative forcing reduces the error in the model's 7-day track forecasts by an average of 27% (∼205 km).

Key Words: Saharan dust; dust-radiative forcing; Hurricane track; dust model

Received 20 October 2014; Revised 6 February 2015; Accepted 20 February 2015; Published online in Wiley Online Library

1. Introduction

Over the past two decades, the scientific community has made significant improvements in forecasting the movement and track of tropical cyclones (TCs). These improvements are due to several factors, including better assimilation of satellite observations, increases in model resolution, and improved physical parameterizations (Rappaport *et al.*, 2009). These factors affect the movement of TCs by changing their structure as well as their synoptic-scale environment. Structural changes can arise from changes in the storm size and intensity, while environmental changes can arise from changes in the synoptic-scale temperature and wind fields.

Structural changes in TCs can occur through a variety of mechanisms, among them changes in cloud microphysics. For example, using idealized simulations based on an initially calm and homogeneous atmosphere, Fovell *et al.* (2010) showed that TC structure is sensitive to cloud microphysics associated with cloud-radiative feedback. The structural changes brought about by the feedback cause changes in the size and the outer winds of the TCs, which, due to differential planetary vorticity advection – termed the beta-gyre effect (Holland, 1983) – cause larger TCs to move more westward.

Changes in the synoptic-scale environment, particularly the steering winds within 500–700 hPa, have also been shown to be a key driver of TC movement (Chan and Gray, 1982). Although forecast errors of the synoptic-scale environment have been reduced in recent years, further improvements in physical parameterizations are still needed, especially on the regional-scale. For example, Torn and Davis (2012) have shown that the inclusion of marine shallow cumulus parameterization in the Advanced Hurricane Weather Research and Forecasting Model (AHW) improved the synoptic-scale flow over the West Atlantic in TC forecasts. The inclusion of the parameterization caused the low- to mid-level temperature and temperature gradient to decrease, which in turn improved the environmental steering flow and thus TC tracks. But their results still showed northeastward, eastward, and southeastward wind biases over the East Atlantic, both before and after the inclusion of marine shallow cumulus parameterization (see their Figure 4). The wind biases are associated with errors in the TC track forecasts over the East Atlantic, a region where additional physics may be needed or existing physics needs to be improved in order to better represent the environmental steering flow (Rodwell and Jung, 2008).

Over the East Atlantic, the African easterly jet (AEJ) is a prominent feature of the synoptic-scale environment that surrounds a TC. The AEJ is a manifestation of thermal wind balance: a strong meridional temperature gradient produced by warm air to the south and hot air to the north results in vertically sheared easterly flow. The AEJ serves not only as an energy source for African easterly waves (AEWs), which are important to the development of TCs in the Atlantic, but also plays an important role in steering storms. Consequently, accurate representation of the AEJ in numerical models is essential for Atlantic TC track forecasts (George and Gray, 1976).

Another prominent feature over the East Atlantic, one that we will show affects the movement of Hurricane *Helene*, is the dust within the Saharan air layer (SAL). The SAL, which originates over the Saharan desert, is a layer of hot, dry air that overlies the cool marine layer of the East Atlantic. Within the SAL, plumes of Saharan mineral dust aerosols occur episodically and are often quite pronounced, particularly during the hurricane season. Laken *et al.* (2014) show that the dust events peak during July to September, which are the primary hurricane months. During these months there are, on average, 28 Saharan dust events. The formation of the dust plumes is driven by dust emission processes that vary seasonally and diurnally and that span the micro-scale to synoptic-scale (Knippertz and Todd, 2012). Winter is dominated by large-scale processes, such as cyclonic storms and Harmattan surges, while summer is more complex and includes dust emission processes associated with AEWs, the Saharan heat low, northward intrusion of the monsoonal circulation, cold-pool outflow linked to mesoscale convective systems, and dust devils. Once the dust is lofted into the atmosphere, it absorbs, scatters and emits radiation, which modifies the energy budget of the atmosphere and surface (Carlson and Benjamin, 1980; Zhu *et al.*, 2007; Chen *et al.*, 2010; Cherian *et al.*, 2010; Zhao *et al.*, 2011). Generally, direct dust-radiation feedbacks modify the energy budget in a way that causes cooling at the surface below the dust plume and heating within the plume, i.e. heating in the lower to middle troposphere.

The change in the energy budget by dust-radiation forcing has been related to a variety of circulation features over West Africa, the East Atlantic, and Europe. These include: decreases in West African monsoon rainfall (Yoshioka *et al.*, 2007; Konare *et al.*, 2008; Solmon *et al.*, 2008; Zhao *et al,* 2011); modulation of hurricane genesis and intensification (Sun *et al.*, 2008); changes in the horizontal temperature gradient near the southern edge of SAL, which, via thermal wind balance, changes the vertical wind shear and thus the intensity and direction of the AEJ (Konare *et al.*, 2008; Chen *et al.*, 2010; Ma *et al.*, 2012); delay in the onset of mesoscale convective system precipitation over Central North Africa (Shi *et al.*, 2014); and improvement in convective cloud rainfall forecasts in Europe (Chaboureau *et al.*, 2011).

The above studies underscore the importance of Saharan mineral dust aerosols to the TC environment. With this in mind, we show in Figure 1 a scenario that describes how Saharan dust can affect TC movement and track over the East-Central Atlantic. In this scenario, a large, dense dust plume originates over North Africa and moves over the East Atlantic. At this time (T_1), the TC is south of the jet and the main part of the plume, where it begins experiencing the plume's diabatic heating and cooling effects (dust-radiative forcing). As the plume is swept farther to the westsouthwest, due to the combined influence of the beta-gyre effect, large-scale circulation, and steering jet, the TC becomes embedded within the plume (T_2), where the dust-radiative forcing causes small changes in the direction and speed of the storm. The small changes accumulate so that as the TC exits the plume (T_3), it has a different trajectory than it would have had in the absence of dust-radiative forcing. Consequently, the difference in the tracks with and without dust-radiative forcing continues to grow with distance from the plume. The numerical simulations that we show later support the scenario illustrated in Figure 1.

To our knowledge, no study has modeled the potentially important role that dust-radiative forcing plays in modulating TC movement over the East-Central Atlantic. Here we use Hurricane *Helene* (2006) as a case study to examine the effects of dust-radiative forcing on its movement. To do so, we begin with a brief analysis based on historical forecasts. The analysis shows a northeastward or southeastward bias in TC track forecasts over the East Atlantic. Motivated by the historical forecasts, we follow with a description of our dust model and an analysis of our numerical results, which are in good agreement with observations. We then close with a brief summary and conclusions.

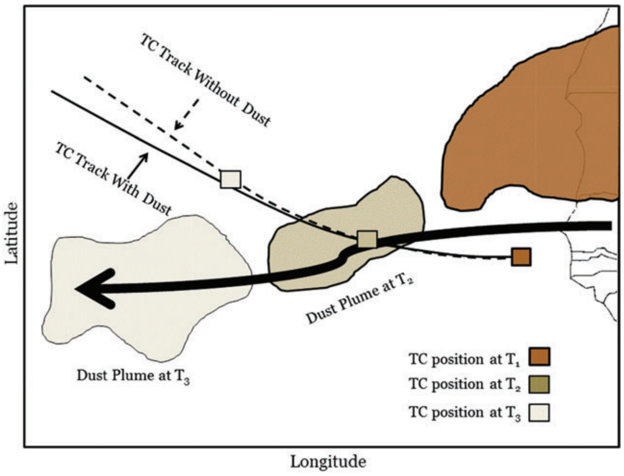

Figure 1. Schematic showing the TC positon along its track at three different times relative to the dust plume position at the same times. Relative concentrations of the dust plumes are denoted by dark brown (high concentration), medium brown (moderate concentration), and light brown (low concentration). At time T_1, the TC is south of the main part of the plume and begins experiencing its diabatic heating and cooling effects. As the plume is swept farther to the westsouthwest by the large-scale circulation and steering jet (bold black arrow), the TC becomes embedded within the plume (T_2), where the dust-radiative forcing causes small changes in the direction and speed of the storm. As the TC exits the plume (T_3), it has a different trajectory than it would have had in the absence of dust-radiative forcing. The difference in the tracks with and without dust-radiative forcing continues to grow with distance from the plume.

2. Model and results

2.1. Motivation

In this section, we provide a brief analysis whose purpose is to motivate our numerical simulations. Our analysis uses historical forecasts to show that, despite recent improvements in TC track forecasts, northeastward and southeastward biases characterize the historical storm track forecasts over the East Atlantic.

Galarneau and Davis (2013) have analyzed 24-h forecasts during the 2008–2010 North Atlantic TC seasons and found an eastward bias in the TC's environmental flow for westward-moving TCs that occurred east of 60°W over the Atlantic. Using an error diagnostic equation, they found that the bias could be reduced by reducing the errors in the environmental wind field. In this section, we confirm the biases found by Galarneau and Davis using their data set. But our analysis differs from theirs in two key aspects. First, we use a 5-day TC track error analysis rather than 24-h. Second, we focus on TCs starting farther east (east of 35°W), i.e. where the influence of dust-radiative forcing on TCs is typically the greatest.

As in Galarneau and Davis (2013), our analysis is based on the National Center for Atmospheric Research (NCAR) 5-day archived TC hindcasts for 2009 and 2010, during which time the genesis of nine TCs occurred over the East Atlantic. The hindcasts are produced by ensemble Kalman filter data assimilation and the AHW, which includes a shallow marine cumulus parameterization (see Torn and Davis, 2012). Due to sedimentation, wet scavenging, and the assimilation of observations, we expect the effect of the dust-radiative forcing on the TC's movement to become less important as the distance from the dust source region increases (Tegen and Fung, 1994). Thus we

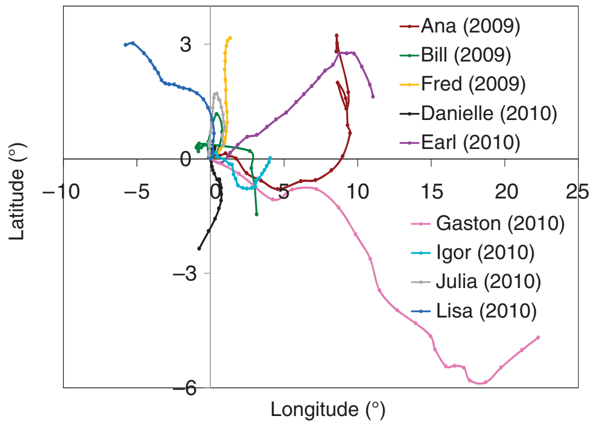

Figure 2. Five-day forecasted track errors for TCs that developed from tropical depressions over the East Atlantic before reaching 35°W for 2009 and 2010. The track error is calculated by subtracting the National Hurricane Center best track position data from forecasts with the correction of the storm's initial position error (i.e. no error at the initial time; the time interval between dots is 6 h). The track errors in the upper right quadrant, for example, mean that storms move too far to the northeast compared with observations. The forecasts are from the National Center for Atmospheric Research.

only consider TCs that became tropical depressions (TDs) over the East Atlantic, i.e. before reaching 35°W. We chose the forecasts that were initialized within 2 days after the storms became TDs and then estimated the average of the forecast track error against the National Hurricane Center best track positions, with the constraint that the initial track error is subtracted throughout the forecast. The forecasts were initialized every 6 h, which provided up to nine forecasts for the average of the track error for each of the nine storms.

Figure 2 shows the 5-day TC track forecast errors for the nine TCs. The errors range from a couple of hundred km to a thousand km. Eight out of the nine reside in the first and forth quadrants of the figure, meaning that they have a northeastward or southeastward track bias, i.e. storms move too far to the northeast or southeast compared to the observations. These results are consistent with Galarneau and Davis (2013).

2.2. *Model*

Numerical simulations of the effects of dust-radiative forcing on Hurricane *Helene* (2006) are carried out using the regional Weather Research and Forecasting (WRF) dust model, similar to that developed by Chen *et al.* (2010) but with a newer version of the WRF model that updates the dust size and distribution. The model is based on WRF V3.2.1 (Skamarock *et al.*, 2008), which uses terrain-following mass coordinates and the Arakawa C grid. To conserve mass and entropy, the governing equations are written in flux form. A third order Runge-Kutta time scheme is used; fifth and third order advection schemes are used for the horizontal and vertical directions, respectively.

The effects of Saharan mineral dust aerosols on the atmospheric circulation depend on the transport, mixing, sources and sinks, and radiative properties of dust. In the WRF dust model, these effects are described by a dust continuity equation, which can be written in flux form as (Chen *et al.*, 2010):

$$\frac{\partial C}{\partial t} = \nabla \bullet \vec{V} C + C_{pbl} + C_{cov} + S_C + E_C, \tag{1}$$

where C is the mass coupled dust mixing ratio (Pa kg kg^{-1}). The first term on the right-hand side of Eq. (1) is the flux divergence of dust (transport); C_{pbl}, C_{cov}, S_C and E_C represent, respectively, sub-grid boundary layer mixing, sub-grid cumulus mixing, dust processes for sedimentation, and sources and sinks. The source in E_C represents surface dust emission that is injected into the model's first half layer (note: the WRF vertical coordinate is staggered); the sink in E_C represents the dry deposition to the ground. In order to relax the numerical time step and avoid numerical instability, a time splitting method is used for the calculation of sedimentation due to the high vertical spatial resolution near the surface. The dust-radiative forcing is included in the thermodynamic equation.

In the WRF dust model, dust emission occurs when the vegetation type is barren, the soil volumetric moisture is less than 0.2, and the 10 m wind speed, u_{10}, exceeds the threshold velocity, u_{10c}. Following Tegen and Fung (1994), the surface dust emission flux, e_c (µg s^{-1} m^{-2}), is chosen proportional to the cube of the wind speed: $e_c = \max\,(\alpha(u_{10} - u_{10c})u_{10}^2, 0)$; α is a dimensional constant, $u_{10c} = 6.0$ m s^{-1}, and $\alpha = 0.4$ µg m^2 s^{-5}. Here we depart from Chen *et al.* (2010) and choose the dust bin-size distribution and the percentage of dust emission flux for each bin based on Kok (2011a). This choice is based on Kok's theoretical analysis, which shows that the emitted dust size distribution reflects a scale-invariant process, such that the size distribution of emitted dust does not change with wind speed, soil moisture, soil type, soil size distribution, etc. Subsequently, Kok (2011b) compared observations from several different field studies and showed that the observational data support his initial hypothesis of scale-invariance in emitted particle size distributions. Thus following Kok (2011a, his equation 5), we use a power-law to calculate the split of the dust mass flux into 12 bin sizes, corresponding to dust diameters of 0.3, 0.7, 1.2, 2, 3, 4, 5, 6, 7, 8, 9, and 10 µm. In the WRF dust model, the 12 bin sizes are carried in a four-dimensional (4D) variable called 'scalar.' The four dimensions are the spatial directions x, y, and z, and the bin size. As in Chen *et al.* (2010), the aerosol optical properties – single-scattering albedo, asymmetry parameter, and extinction coefficient – are calculated for different wavelengths using the Optical Properties of Aerosols and Cloud (OPAC) software package (Hess *et al.*, 1998). OPAC only has three modes of mineral dust (nucleation, accumulation, and coagulation). The 12 bins of dust are lumped into the three modes, keeping the mass conserved when calculating optical properties for each of the shortwave and longwave bands (see table 2 in Chen *et al.*, 2010). The dust-radiation interaction is implemented into the National Aeronautics and Space Administration (NASA)/Goddard Space Flight Center (GSFC) shortwave and longwave radiation schemes (Chou and Suarez, 1999; Chou *et al.*, 2001).

2.3. *Experimental designs*

For our numerical experiments we chose Hurricane *Helene* (2006) as a case study because it was accompanied by a moderate dust plume along part of its track. *Helene* began as an African tropical wave with a broad area of low pressure. The wave departed the West African coast on 11 September and was accompanied by a dust plume having an aerosol optical depth (AOD) of ∼1.3, which is typical of the modest plumes observed over the West African coast (see Figure 3(a)). *Helene* was classified as a tropical depression at 1200 UTC on 12 September and as a hurricane at 1200 UTC on 16 September. Rapid intensification occurred between 1200 UTC on 17 September and 0600 UTC on 18 September. The storm first moved towards the westnorthwest and then shifted slightly towards the northwest after 15 September.

We conducted six numerical experiments to investigate the effects of dust-radiative forcing on *Helene*'s track forecasts (see Table 1). The experiments are combinations of the activation or deactivation of dust-radiative forcing, denoted by DA and DD, respectively, and three different microphysics schemes: (i) the Purdue Lin microphysics scheme developed by Chen and Sun (2002; PL); (ii) the WRF single-momentum 6-class microphysics scheme developed by Hong and Lim (2006; W6); and (iii) the two moment microphysics scheme developed by Cheng *et al.* (2010; TM). Both PL and W6 are single-moment bulk microphysics schemes. W6 includes five species – water vapor, cloud water, rain, ice, and snow; PL includes an additional

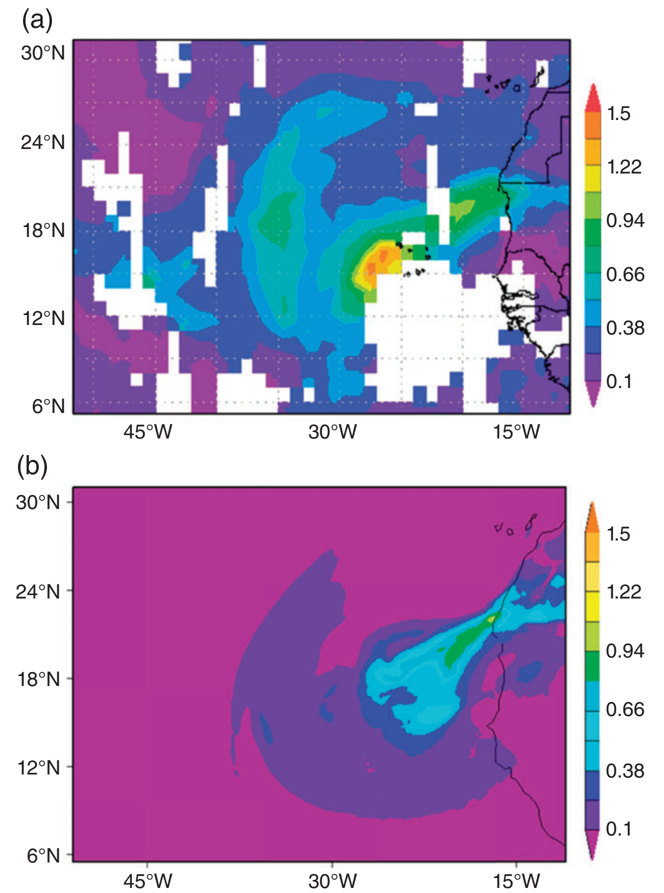

Figure 3. (a) Observed AOD (unitless; shading) at 550 nm on 12 September 2006; (b) averaged 36-h simulated AOD at 550 nm from three experiments with the activation of dust-radiative forcing (ON; i.e. the average from PL-DA, W6-DA, and TM-DA) at 1200 UTC on 12 September. The missing data over the region surrounding 12°N and 22°W is due to clouds associated with Hurricane *Helene*. The AOD data, with a horizontal resolution of 1° × 1°, are obtained by the Moderate Resolution Imaging Spectroradiometer (MODIS) and the Multi-angle Imaging SpectroRadiometer (MISR) instruments. MISR is on the *Terra* satellite; MODIS is on both the *Aqua* and *Terra* satellites.

Table 1. The six numerical experiments, which are combinations of dust-radiation activation or dust-radiation deactivation and three different microphysics schemes.

Experiment	*Microphysics scheme*	*Dust-radiation activation*
PL-DA	Purdue Lin (PL) scheme	Yes (DA)
PL-DD	Purdue Lin (PL) scheme	No (DD)
W6-DA	WSM 6-class (W6) graupel scheme	Yes (DA)
W6-DD	WSM 6-class (W6) graupel scheme	No (DD)
TM-DA	Cheng two-momentum microphysics (TM) scheme	Yes (DA)
TM-DD	Cheng two-momentum microphysics (TM) scheme	No (DD)

AOD measures the vertically integrated extinction by aerosols. During the hurricane season, dust is the major contributor to the AOD measurements over the Sahara Desert and the East Atlantic.

species – graupel. A one-moment scheme has one prognostic variable for each species (i.e. mass), while a two-moment scheme has two prognostic variables (i.e. mass and the number concentration). This is the first study to implement the Cheng *et al.* two-moment microphysics scheme (TM) into the WRF dust model. Like the Purdue Lin scheme, the TM scheme also includes six species. We have chosen three different microphysics schemes for two reasons. First, we want to demonstrate that the effects of dust-radiative forcing on *Helene*'s movement are robust. And second, the three microphysics schemes are the only ones that do not use the 4D variable 'scalar' in WRF V3.2.1. This is important because 'scalar' is used to carry the 12 dust fields in the WRF dust model and cannot be shared with another variable with different properties. The remaining physics schemes in the WRF dust model include the Medium Range Forecast (MRF) boundary layer parameterization (Hong and Pan, 1996); the Kain-Fritsch (KF) cumulus parameterization (Kain, 2004); and the Goddard Space Flight Center (GSFC) longwave and shortwave radiation schemes (Chou and Suarez, 1999; Chou *et al.*, 2001). The KF and MRF schemes account for the dust physical processes associated with mixing in the cumulus parameterization and boundary layer parameterization, respectively.

For each experiment, three domains with two-way interaction are configured. The horizontal grid spacing for domains 1–3 are 36, 12, and 4 km, respectively. The vertical grid spacing is stretched

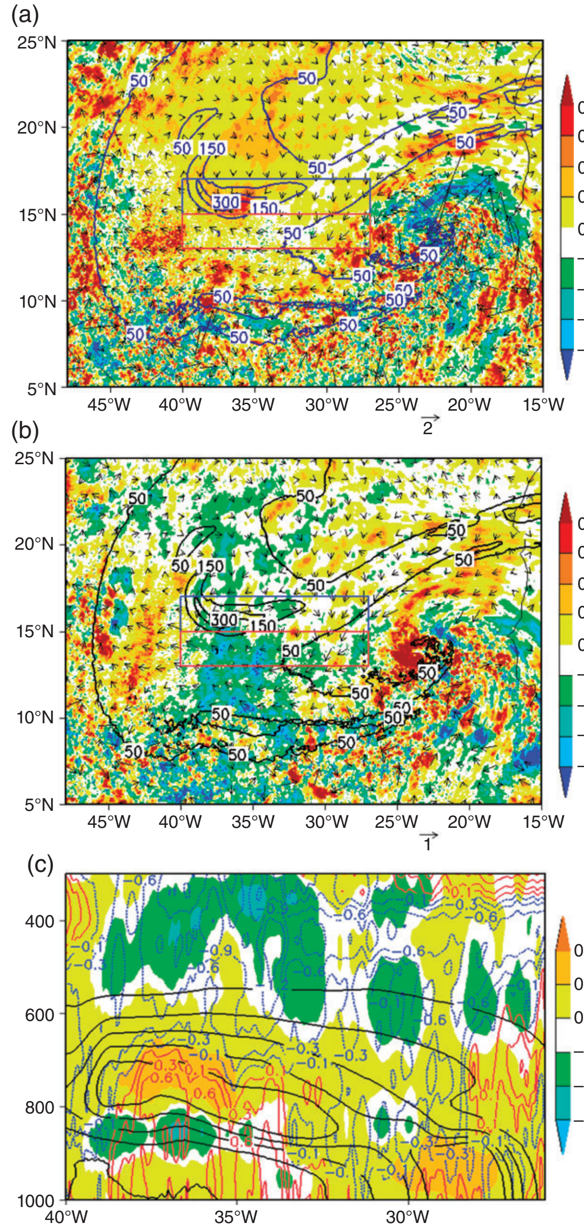

Figure 4. The horizontal cross-section of differences between ON and OFF in (a) 750 hPa potential temperature (K; shading) and the vertical wind shear vectors between 600 and 900 hPa and (b) 450 hPa potential temperature (K; shading) and deep layer steering wind vectors between 850 and 200 hPa. The black contours in (a) and (b) are 750 hPa total dust ($\mu g\ kg^{-1}$) from experiments with dust-radiative forcing (ON). Note that in (b) the differences of the deep layer steering wind vectors greater than 1 $m\ s^{-1}$ are set to missing data for easier visualization. (c) The vertical cross-section of differences between ON and OFF (ON-OFF) in band-averaged temperature (K; shaded; averaged between 15 and 17°N in the blue box area in (a) and (b)) and zonal wind speed (blue dashed contours for negative and red contours for positive; $m\ s^{-1}$; averaged between 13 and 15°N in the red box area in (a) and (b)). All figures are plotted at 1200 UTC on 13 September 2006 (60-h forecast). The black contours in (c) represent the total band-averaged (15–17°N) dust ($\mu g\ kg^{-1}$) from ON and the dust contours start from 10 $\mu g\ kg^{-1}$ with an interval of 50 $\mu g\ kg^{-1}$.

with a resolution of 30 m near the surface to about 1 km near the model top. Domain 3 covers the East Atlantic, the primary region of interest for our study. The initial and boundary conditions are from the National Centers for Environmental Prediction (NCEP) Global Forecast System Final analysis (FNL) with a horizontal spatial resolution of $1^\circ \times 1^\circ$ and a temporal resolution of 6 h. The model was integrated forward in time for 7 days, starting from 0000 UTC on 11 September 2006, which is 36 h before *Helene* was classified as a TD. A time step of 120 s was used for domain 1.

To provide the dust field in the model initial conditions, a 3-day WRF simulation from 0000 UTC on 8 September to 0000 UTC on 11 September 2006 was conducted. The domain configuration is the same as stated above, except only the first two domains are used. To provide a better distribution of dust, we applied, for the entire 3-day simulation, four-dimensional data assimilation (nudging) to the state variables (e.g. wind, temperature, etc.), except for dust. The 12-bin dust fields at the end of the 3-day simulation are then imported into the dust initial conditions for each of the six numerical experiments. Recall, the meteorological initial and boundary conditions for the six experiments are from FNL data.

2.4. Results

To investigate the effects of dust-radiative forcing on *Helene*'s track forecasts, we divided the simulations into two groups, denoted by ON and OFF. ON represents the average from three experiments with the activation of dust-radiative forcing (PL-DA, W6-DA, and TM-DA), while OFF represents the average from the other three simulations with the deactivation of dust radiative forcing (PL-DD, W6-DD, and TM-DD). We first compare simulated AOD with satellite retrieved data to evaluate model performance on the dust forecasts. After a 36-h integration, the model slightly underestimates the AOD value and the simulated dust plume propagates slower than observations (compare Figure 3(a) and Figure 3(b)). This implies that either the intensity of the AEJ might be underestimated or the dust does not reach high enough where the easterly wind is stronger, or both. Nevertheless, the pattern of the dust plume is well captured and the order of the AOD magnitude is reasonably forecasted.

We next evaluate the simulated dust mass concentration at the model first half level with surface observations in Jeong *et al.* (2008). The surface observations of the dust mass concentration were collected at Sal Island, Cape Verde (16.7°N, 22.9°W) during the NASA African Monsoon Multidisciplinary Analyses (NAMMA) field experiment. The dust mass concentration increased and then decreased during 12–13 September 2006 (figure 2c in Jeong *et al.*, 2008). This occurred when the southern edge of the dust plume passed Sal. The WRF dust model captures very well the time period when the dust mass concentration was elevated (figure not shown). The model values, however, are about two to three times the observations (200 versus 80 $\mu g\,kg^{-1}$). The difference between the model values and the observations may be due to the neglect of dust wet scavenging or other dust parameterizations, such as the dust size distribution and dust sedimentation. Because the pattern of the dust plume is well captured and the orders of magnitude of the AOD and dust mass concentration are reasonably forecasted, the model can be used to study the effects of dust-radiative forcing on *Helene*'s track forecasts. We note that the missing data over 15–30°W and 6–15°N in the observed AOD is due to the presence of clouds.

Dust-radiative forcing directly changes the energy budget of the atmosphere and at the surface. This produces changes in the temperature gradient surrounding the dust plume, which in turn modifies the wind speed, direction and vertical shear. These changes are evident in Figure 4(a), which shows the differences between 750 hPa average potential temperature and vertical wind shear (horizontal wind at 600 hPa minus horizontal wind at 900 hPa) between ON and OFF at 1200 UTC on 13 September 2006. This time corresponds to 24 h after the storm became a TD or, equivalently, 60 h after model integration began. Figure 4(a) clearly shows a dust-induced warm anomaly within the plume; the maximum is about 0.4 K. South of the dust plume (5–10°N), the warming and cooling becomes random, which is partly associated with individual convective features. The difference in the vertical wind shear between ON and OFF over the storm area (17–25°W and 10–15°N) is large and unorganized compared to the vertical wind shear over the dust plume area. The large difference in shear over the storm area results from the fact that the storm has a strong wind field, so that any change in the storm position or structure can produce a large change in the wind. By contrast, around the maximum of the plume, the wind shear difference is organized and clockwise, consistent with the thermal wind relationship wherein a warm anomaly lies to the right of the vertical shear difference direction.

Figure 4(c) shows the vertical cross-section of band-averaged potential temperature and zonal wind speed differences between ON and OFF, and the total dust field from ON. The potential temperature difference and the dust field are averaged for the region of the middle level dust maximum (15–17°N). Because the wind shear responds to the temperature gradient rather than the temperature itself, the wind speed is averaged for the region south of the middle level dust maximum (13–15°N). Dust concentrations greater than 10 $\mu g\,kg^{-1}$ extend just above 600 hPa. At lower levels, the easterly wind in some regions weakens (red solid contours) and slightly strengthens in others (blue dashed lines). This is because the low-level potential temperature difference is quite complicated over the region 15–17°N, which is near the northern edge of the low-level dust plume (figure not shown). Diagnosis of the forcing terms in the thermodynamic equation indicates that the advection, boundary layer mixing, and radiative forcing all contribute to the complicated potential temperature difference. At mid-levels, the easterly wind becomes stronger, consistent with

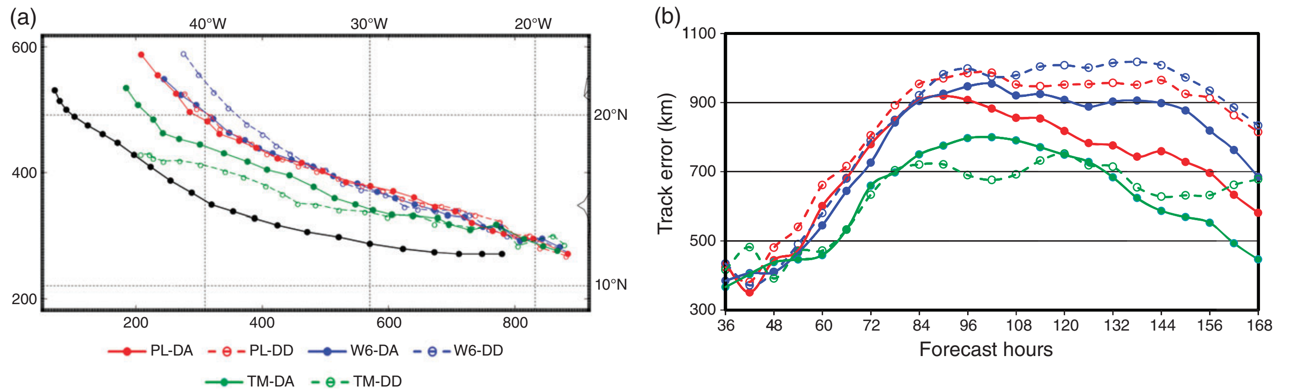

Figure 5. (a) Observed (black solid line) and simulated *Helene*'s tracks; (b) simulated track errors from 1200 UTC on 12 September to 0000 UTC on 18 September 2006. The blue, red, and green colors represent the WSM6, Purdue Lin, and the two-moment microphysics schemes. The solid and dashed lines are experiments with and without dust-radiative forcing, respectively.

the increase of the easterly vertical wind shear anomaly shown in Figure 4(a). There is a cooling difference above the dust plume between 33 and 40°W (Figure 4(b,c)), which is not persistent. The cooling is partially due to the potential temperature advection (figure not shown). However, because the pattern of the potential temperature difference keeps changing, the air above the dust plume is unable to adjust to thermal wind balance. While the potential temperature change due to the dust forcing stops at about 600 hPa, the wind difference between ON and OFF is still clockwise, but is weaker and decreases with height above 600 hPa. As a result, the difference of the deep layer steering flow, which is defined as the wind average between 850 and 200 hPa (Galarneau and Davis, 2013), is clockwise (Figure 4(b)), similar to that of the vertical shear wind difference (Figure 4(a)). The implication is that the change of the storm's track, shown later in Figure 5, is very likely due to the change in the deep layer steering flow.

Although the difference in the wind and its vertical shear between ON and OFF are small surrounding the dust plume, the small dust-induced difference in the environmental wind continuously operates on the TC as it transits the dust plume, causing the TC to exit the plume with a different trajectory than it would have had in the absence of dust-radiative forcing. This scenario is consistent with Figure 1 and borne out in the numerical simulations shown later in Figure 6. We note that the storm's speed and direction and the size of a dust plume can influence the amount of time it takes the storm to transit the dust plume. As a consequence, the dust-radiative effect on TC motion will be less for a faster moving storm, a smaller dust plume, or both.

Figure 5(a) shows the observed and forecasted storm tracks for each of the six experiments starting from the 36-h forecast, which corresponds to the initial time of the TC formation. The OFF experiments (W6-DD, PL-DD, TM-DD), where the dust-radiative feedbacks are deactivated, clearly show, like Fovell *et al.* (2010), the sensitivity of the tracks to the different microphysics schemes. But in sharp contrast to the study of Fovell *et al.* , which was based on idealized simulations with no environmental wind, we consider a real case where the storm movement is dominated by the environmental steering flow (AEJ), which is strong and complicated over the region of interest (East Atlantic). Thus in our case it is difficult to clearly distinguish the impact of the microphysics schemes on the storm tracks, a problem that is beyond the scope of this study. Most importantly, however, Figure 5(b) shows that irrespective of the microphysics scheme, the dust-radiative feedback reduces the track errors. For example, compare W6-DD with W6-DA. In this pair of experiments, the dust-radiative feedback begins to reduce the track error after ~48 h of integration, corresponding to a 12-h forecast after the TC formed; by 84 h of integration, the track error is reduced even more after the correction of the track trajectory. At the end of the 7-day (168-h) forecast, the track error is reduced by ~149 km (~17.8%). For the PL microphysics scheme, the PL-DD and PL-DA simulations yield similar track trajectories, but the TC moves faster along the PL-DA track. At the end of the 7-day forecast, the dust-radiative feedback reduces the track error by ~234 km (~28.7%). For the TM microphysics scheme, the TM-DD track is relatively poor, evidenced by a trajectory that is too far to the west. The inclusion of the dust-radiative forcing (TM-DA) effectively corrects the TC's moving direction, resulting in the best trajectory among all of the experiments. After the 7-day integration, the dust-radiative feedback reduces the track error by ~232 km (~34.2%). The average reduction in the track error for the forecasts is ~205 km (27%).

To illustrate further the effects of dust-radiative forcing on the forecasted storm tracks, we show in Figure 6, for the W6 microphysics scheme at three different times, the dust plume superimposed on the forecasted tracks for W6-DD and W6-DA. Figure 6(a) shows that at 36 h, when *Helene* first becomes a tropical depression, it is accompanied by a moderate dust plume to the northwest. By 84 h (Figure 6(b)), the storm is moving westnorthwest, while the plume continues to move west

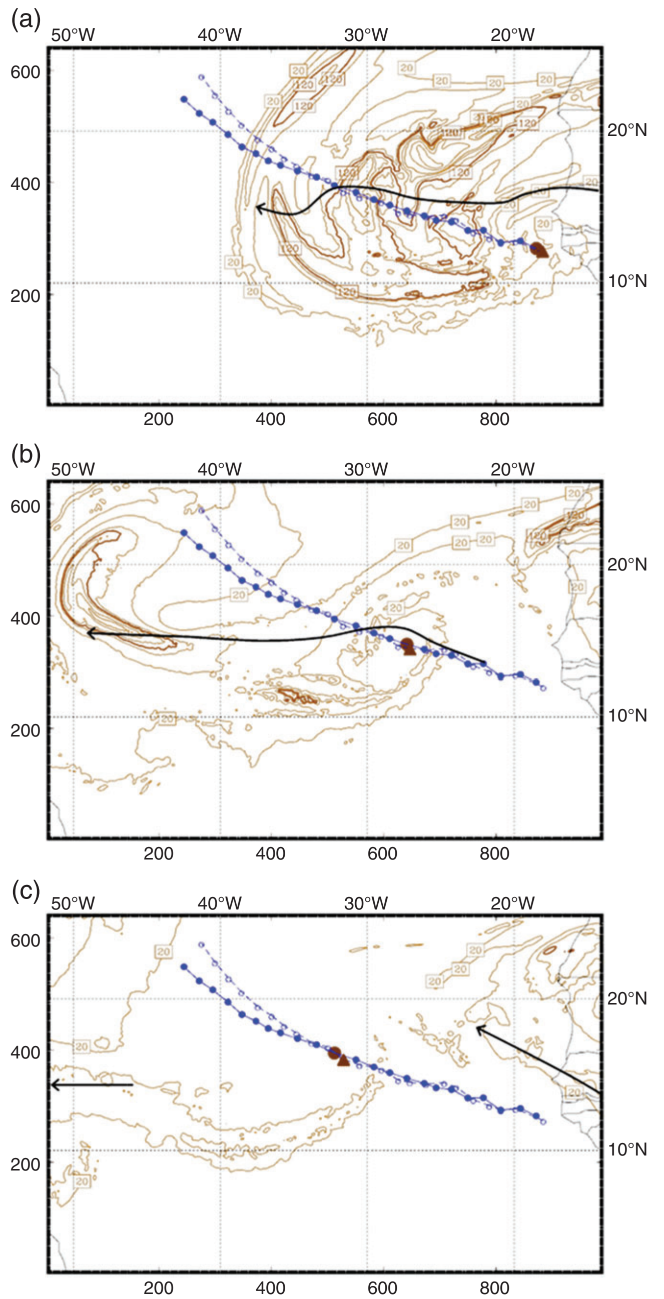

Figure 6. The 750 hPa total dust distribution (contours; μg kg^{-1}) for W6-DA at (a) 36 h, (b) 84 h and (c) 108 h, which correspond, respectively, to 0, 48, and 72 h after the TC formed. The light brown contours start from 20 μg kg^{-1} with a smaller interval of 40 μg kg^{-1} until 220 μg kg^{-1} and then a larger interval of 100 μg kg^{-1}. The thicker brown contour highlights the total dust value of 120 μg kg^{-1}. Superimposed on the dust distribution are the forecasted tracks for *Helene* for W6-DA (solid blue line) and W6-DD (dashed blue line). The brown dot and triangle in each panel are the storm locations for W6-DA and W6-DD, respectively, at the time of the dust plume distribution shown in the figure. Also shown at that time is the location of the 750 hPa jet (indicated by black arrows).

following the jet (denoted by arrow). *Helene* crosses the dust plume in about 2–3 days. During this time, the dust-radiative forcing causes clockwise vertical wind shear and clockwise deep layer steering flow anomalies along the plume. South of the plume the dust-radiative forcing produces a northeast, east, to southeast deep layer steering flow anomaly, while to the north of the plume the forcing produces a northwest, west, to southwest deep layer steering flow anomaly. It is important to keep in mind, however, that the impact of the dust-radiative forcing on the TC's movement is reduced as distance from the dust source region increases. Thus the dust-modulated storm experiences stronger easterly anomalies at the beginning of its track and much weaker westerly anomalies later. Once the storm has passed through the major dust region, i.e. after the 108-h forecast (Figure 6(c)), the storm's location forecast and its track trajectory (W6-DA) are much better than the dust-radiation deactivation forecast (W6-DD) (see Figures 5(b) and 6(c)). The results shown in Figure 6 are consistent with the scenario presented in Figure 1.

3. Summary and conclusions

This is the first study to model the effects of direct dust-radiative forcing on the track of a hurricane. Using Hurricane *Helene* (2006) as a case study, the Weather Research and Forecasting dust model was used to examine the diabatic heating effects produced by Saharan mineral dust aerosols on *Helene*'s track over the East-Central Atlantic Ocean. We chose *Helene* as a case study because it was accompanied along part of its track by a moderate dust plume typical of those observed over the West African coast.

To motivate our numerical experiments, we carried out an analysis using 2 years of tropical cyclone (TC) hindcast data. We showed that despite recent improvements in tropical cyclone (TC) track forecasts, track forecasts over the East Atlantic are characterized by northeastward and southeastward biases.

Our modeling investigation of the effects of Saharan dust on the track of *Helene* hinged on six numerical experiments. These experiments were combinations of the activation or deactivation of dust-radiative forcing and three different microphysics schemes. We showed that the model-generated dust plume modifies the thermal field, causing a clockwise turning of the vertical shear surrounding the plume, which modulates *Helene*'s moving speed and direction. While the storm transits the plume, the dust-radiative forcing causes small changes in the moving speed and direction of the storm. Although the differences in the steering wind are relatively small, the time-integrated effect is such that *Helene* exits the plume on a different trajectory than it would have had in the absence of dust-radiative forcing. Consequently, the difference in the tracks with and without dust-radiative forcing continues to grow beyond the edge of the plume. Irrespective of the microphysics scheme, the dust-radiative forcing improves *Helene*'s track forecast; the error in the model's 7-day track forecasts is reduced by an average of 27% (∼205 km).

We have shown that the effects of Saharan mineral dust aerosols on the track forecast of Hurricane *Helene* are robust and important. But additional work is needed to improve the accuracy of the dust-radiative forcing in numerical models, including dust emission processes, particle size distributions, and optical characteristics, which will require additional direct dust observations. Moreover, additional TCs need to be examined in order to address unresolved questions that were beyond the scope of this study. For example, how frequent are the northeast and southeast biases in TC track forecasts over the East Atlantic related to the presence of dust plumes? How can dust-microphysics interaction change TC development and storm track? What are the track sensitivities to dust plumes characterized by different concentrations and different areal coverage? How does the time needed for the TC to transit the dust plume affect its track? And how is the track affected by the spatial relationship between the environmental wind field, TC circulation, and dust plume? We are currently addressing these questions.

Acknowledgements

The authors thank Dustin Grogan and two anonymous reviewers for their insightful comments on the manuscript. Several data sources were used in this study: FNL data produced by the National Centers for Environmental Prediction (NCEP), which is available at the Computational and Information Systems Laboratory at the National Center for Atmospheric Research (NCAR); daily aerosol optical depth (AOD) data produced by the Giovanni online data system, which is developed and maintained by the NASA Goddard Earth Sciences Data Information Services Center (GES DISC); and TC best track data obtained from the National Hurricane Center/National Oceanic and Atmospheric Association [NHC/NOAA; (http://www.nhc.noaa.gov/data/)]. This work is supported by the NASA Hurricane Science Research Program (grant NNX09AC38G; S.-H. Chen); the NASA High-End Computing (HEC) Program through the NASA Advanced Supercomputing (NAS) Division at Ames Research Center (SMD-13-3895); NSF (Grant 1321720; S.-H. Chen and T. R. Nathan); Scientific Discovery through Advanced Computing (SciDAC) program funded by US Department of Energy Office of Advanced Scientific Computing Research and Office of Biological and Environmental Research (Yi-Chin Liu). The Pacific Northwest National Laboratory (PNNL) is operated by the DOE by Battelle Memorial Institute under contract DE-AC06-76RLO 1830.

References

Carlson TN, Benjamin SG. 1980. Radiative heating rates for Saharan dust. *J. Atmos. Sci.* **37**: 193–213.

Chaboureau JP, Richard E, Pinty JP, Flamant C, Di Girolamo P, Kiemle C, Behrendt A, Chepfer H, Chiriaco M, Wulfmeyer V. 2011. Long-range transport of Saharan dust and its radiative impact on precipitation forecast: A case study during the Convective and Orographically-induced Precipitation Study (COPS). *Q. J. R. Meteorol. Soc.* **137**: 236–251.

Chan JCL, Gray WM. 1982. Tropical cyclone movement and surrounding ?ow relationships. *Mon. Weather Rev.* **110**: 1354–1374.

Chen SH, Sun WY. 2002. A one-dimensional time-dependent cloud model. *J. Meteorol. Soc. Jpn.* **80**: 99–118.

Chen SH, Wang SH, Waylonis M. 2010. Modification of Saharan air layer and environmental shear over the eastern Atlantic Ocean by dust-radiation effects. *J. Geophys. Res.* **115**: D21202, doi: 10.1029/2010JD014158.

Cheng CT, Wang WC, Chen JP. 2010. Simulation of the effects of increasing cloud condensation nuclei on mixed-phase clouds and precipitation of a front system. *Atmos. Res.* **96**: 461–476.

Cherian R, Venkataraman C, Kumar A, Sarin MM, Sudheer AK, Ramachandran S. 2010. Source identification of aerosols influencing atmospheric extinction: Integrating PMF and PSCF with emission inventories and satellite observations. *J. Geophys. Res.* **115**: D22212, doi: 10.1029/2009JD012975.

Chou MD, Suarez MJ. 1999. *A Solar Radiation Parameterization for Atmospheric Studies*, NASA Technical Memorandum 104606, Vol. 15. NASA Goddard Space Flight Center: Greenbelt, MD.

Chou MD, Suarez MJ, Liang XZ, Yan MMH. 2001. *A Thermal Infrared Radiation Parameterization for Atmospheric Studies.* NASA Technical Memorandum 104606, Vol. 19. NASA Goddard Space Flight Center: Greenbelt, MD.

Fovell RG, Corbosiero KL, Seifert A, Liou KN. 2010. Impact of cloud-radiative processes on hurricane track. *Geophys. Res. Lett.* **37**: L07808, doi: 10.1029/2010GL042691.

Galarneau TJ Jr., Davis CA. 2013. Diagnosing forecast errors in tropical cyclone motion. *Mon. Weather Rev.* **141**: 405–430.

George JE, Gray WM. 1976. Tropical cyclone motion and surrounding parameter relationships. *J. Appl. Meteorol.* **15**: 1252–1264.

Hess M, Kopke P, Schult I. 1998. Optical properties of aerosols and clouds: The software package OPAC. *Bull. Am. Meteorol. Soc.* **79**: 831–844.

Holland GJ. 1983. Tropical cyclone motion: Environmental interaction plus beta effect. *J. Atmos. Sci.* **40**: 328–342.

Hong S-Y, Lim JOJ. 2006. The WRF single-moment 6-class microphysics scheme (WSM6). *J. Korean Meteorol. Soc.* **42**: 129–151.

Hong S-Y, Pan H-L. 1996. Nonlocal boundary layer vertical diffusion in a medium-range forecast model. *Mon. Weather Rev.* **124**: 2322–2339.

Jeong MJ, Tsay SC, Ji Q, Hsu NC, Hansell RA, Lee J. 2008. Ground-based measurements of airborne Saharan dust in marine environment during the NAMMA field experiment. *Geophys. Res. Lett.* **35**: L20805, doi: 10.1029/2008GL035587.

Kain JS. 2004. The Kain-Fritsch convective parameterization: An update. *J. Appl. Meteorol.* **43**: 170–181.

Knippertz P, Todd MC. 2012. Mineral dust aerosols over the Sahara: Meteorological controls on emission and transport and implication for modeling. *Rev. Geophys.* **50**: RG1007/2012.

Kok JF. 2011a. A scaling theory for the size distribution of emitted dust aerosols suggests climate models underestimate the size of the global dust cycle. *Proc. Natl. Acad. Sci. U.S.A.* **108**: 1016–1021.

Kok JF. 2011b. Does the size distribution of mineral dust aerosols depend on the wind speed at emission. *Atmos. Chem. Phys.* **11**: 10149–10156.

Konare A, Zakey AS, Solmon F, Giorgi F, Rauscher S, Ibrah S, Bi X. 2008. A regional climate modeling study of the effect of desert dust on the West African monsoon. *J. Geophys. Res.* **113**: D12206, doi: 10.1029/2007JD009322.

Laken BA, Parviainen H, Palle E, Shahbaz T. 2014. Saharan mineral dust outbreaks observed over the north atlantic island of la palma in summertime between 1984 and 2012. *Q. J. R. Meteorol. Soc.* **140**: 1058–1068.

Ma P-L, Zhang K, Shi JJ, Matsui T, Arking A. 2012. Direct radiative effect of mineral dust on the development of African Easterly waves in late summer, 2003–07. *J. Appl. Meteorol. Climatol.* **51**: 2090–2104, doi: 10.1175/JAMC-D-11-0215.1.

Rappaport EN, Franklin JL, Avila LA, Baig SR, Beven JL II, Blake ES, Burr CA, Jiing J-G, Juckins CA, Knabb RD, Landsea CW, Mainelli M, Mayfield M, McAdie CJ, Pasch RJ, Sisko C, Steward SR, Tribble AN. 2009. Advances and challenges at the National Hurricane Center. *Weather and Forecasting* **24**: 395–419.

Rodwell MJ, Jung T. 2008. Understanding the local and global impacts of model physics changes: An aerosol example. *Q. J. R. Meteorol. Soc.* **134**: 1479–1497.

Shi JJ, Matsui T, Tao WK, Tan Q, Peters-Lidard C, Chin M, Pickering K, Guy N, Lang S, Kemp EM. 2014. Implementation of an aerosol–cloud-microphysics–radiation coupling into the NASA unified WRF: Simulation results for the 6–7 August 2006 AMMA special observing period. *Q. J. R. Meteorol. Soc.* **140**: 2158–2175, doi: 10.1002/qj.2286.

Skamarock WC, Klemp JB, Dudhia J, Gill DO, Barker DM, Duda MG, Huang X-Y, Wang W, Powers JG. 2008. 'A description of the advanced research WRF version 3', NCAR technical note NCAR/TN-475+STR, 10.5065/D68S4MVH. NCAR: Boulder, CO.

Solmon F, Mallet M, Elguindi N, Giorgi F, Zakey A, Konaré A. 2008. Dust aerosol impact on regional precipitation over western Africa, mechanisms and sensitivity to absorption properties. *Geophys. Res. Lett.* **35**: L24705, doi: 10.1029/2008GL035900.

Sun D, Lau KM, Kafatos M. 2008. Contrasting the 2007 and 2005 hurricane seasons: Evidence of possible impacts of Saharan dry air and dust on tropical cyclone activity in the Atlantic basin. *Geophys. Res. Lett.* **35**: L15405, doi: 10.1029/2008GL034529.

Tegen I, Fung I. 1994. Modeling of mineral dust in the atmosphere: Sources, transport, and optical thickness. *J. Geophys. Res.* **99**: 22897–22914.

Torn RD, Davis CA. 2012. The influence of shallow convection on tropical cyclone track forecasts. *Mon. Weather Rev.* **140**: 2188–2197.

Yoshioka M, Mahowald NM, Conley AJ, Collins WD, Fillmore DW, Zender CS, Coleman DB. 2007. Impact of desert dust radiative forcing on sahel precipitation: Relative importance of dust compared to sea surface temperature variations, vegetation changes, and greenhouse gas warming. *J. Clim.* **20**: 1445–1467.

Zhao C, Liu X, Leung R, Hagos S. 2011. Radiative impact of mineral dust on monsoon precipitation variability over West Africa, *Atmos. Chem. Phys.* **11**: 1879–1893.

Zhu A, Ramanathan V, Li F, Kim D. 2007. Dust plumes over the Pacific, Indian, and Atlantic oceans: Climatology and radiative impact. *J. Geophys. Res.* **112**: D16208, doi: 10.1029/2007JD008427.